processes

MDPI

Article

Robust Economic Management Strategy for Power Systems Considering the Participation of Virtual Power Plants

Xin Li [1,*], Chen Zhang [2], Qianqian Yi [3] and Jingwei Xu [4,*]

[1] College of Economics & Management, China Three Gorges University, Yichang 443002, China
[2] State Grid Energy Research Institute Co., Ltd., Beijing 102200, China; zhangchen1@sgeri.sgcc.com.cn
[3] Bishan Power Supply Branch of State Grid Chongqing Electric Power Company, Chongqing 402760, China; qianqqian123@163.com
[4] College of Electrical Engineering and New Energy, China Three Gorges University, Yichang 443002, China
* Correspondence: lx13142024@163.com (X.L.); xujw678@163.com (J.X.)

Abstract: The rapid development of new energy technologies and the randomness and intermittency of renewable energy sources, coupled with the complexity of demand-side response, have posed higher requirements for the security and scheduling of power grids. The virtual power plant (*VPP*), as an innovative energy management model, effectively enhances the flexibility and economy of the power system by integrating distributed energy resources and demand-side response resources to participate in the power market and grid operation as a virtual entity. This paper proposes a robust economic management strategy for power systems considering the participation of *VPP*s. Firstly, the uncertainty of renewable energy output is characterized through prediction deviations. Subsequently, the economic dispatch and constraints of *VPP*s are established. Considering the nonlinear characteristics of the model, an improved ant lion optimizer (ALO) algorithm is adopted to ensure optimal solutions. Finally, the effectiveness and feasibility of the proposed method are validated through a case study, using an improved IEEE 30-bus test system. Compared to other methods, the economic income can be increased by up to 3.2%, and the calculation time is only 12.5% of that required for scenario screening-based stochastic optimization. After introducing the carbon trading mechanism, carbon emissions are reduced by 27.7%. The proposed method achieves the goal of maximizing economic benefits while ensuring the secure and stable operation of the power grid.

Keywords: renewable energy sources; virtual power plant (*VPP*); economic management strategy; improved ant lion optimizer (ALO) algorithm

check for updates

Academic Editors: Dimitris Ipsakis and Andreas Yiotis

Received: 11 November 2024
Revised: 19 December 2024
Accepted: 20 December 2024
Published: 26 December 2024

Citation: Li, X.; Zhang, C.; Yi, Q.; Xu, J. Robust Economic Management Strategy for Power Systems Considering the Participation of Virtual Power Plants. *Processes* **2025**, *13*, 25. https://doi.org/10.3390/pr13010025

Copyright: © 2024 by the authors. Licensee MDPI, Basel, Switzerland. This article is an open access article distributed under the terms and conditions of the Creative Commons Attribution (CC BY) license (https://creativecommons.org/licenses/by/4.0/).

1. Introduction

With the shortage of fossil fuels and the deterioration of the ecological environment, various renewable and clean energy sources have garnered significant attention. Among them, wind power generation, backed by rapid technological advancements and superior cost-effectiveness, has received strong support from countries around the world and has become one of the main energy sources in power systems [1]. However, the randomness and intermittency of wind power output adversely affect the secure and economic operation of the system. Relying solely on conventional units to mitigate this randomness may lead to frequent start-ups and shut-downs, or significant increases and decreases in output, thereby increasing the difficulty of scheduling and operation. Hence, there is an urgent need for demand-side resources to participate in scheduling [2]. The virtual power plant (*VPP*), by aggregating distributed energy resources and adjustable loads, enhances its operational

stability and promotes the integration of renewable energy. As a new distributed energy grid connection technology, the *VPP* can mitigate the impact of the randomness of wind and solar power output by optimizing unit output and tapping into the adjustment potential of controllable loads, thereby ensuring smooth system operation [3].

In the early stages of its development, the virtual power plant (*VPP*) primarily served as a means of connecting single-type distributed energy resources to the grid. The concept of the *VPP* originated from the notion of "virtual public utilities" proposed by Dr. Shimon in 1997, which emphasized the use of flexible cooperation methods by non-asset entities, driven by market forces, to provide specific public services to consumers [4]. "Virtual" and "service customization" are the main characteristics of the *VPP*. Based on the type of resource management and control within the *VPP*, early *VPP*s aggregated distributed generation resources to form power-type *VPP*s, providing voltage support services to medium voltage distribution networks [5]. To further facilitate the transition from "source following load" to "source–load interaction", references [6,7] aggregated wind and solar power generation resources with loads to form source–load-type *VPP*s with defined regulation capacity and ramp rates, participating in day-ahead unit commitment regulation services. To further define the *VPP*, references [8–10] view it as a combination of controllable resources and flexible control technologies. In terms of positioning, the *VPP* is mainly intended to support the reliable integration of distributed generation (DG) [11], overcoming the fluctuations and randomness of DG output in power supply balance adjustments, and thus providing a medium for DG to participate in power market transactions.

The key to the involvement of virtual power plants (*VPP*s) in power system dispatch lies in accurately describing user behavior through physical and mathematical modeling, based on factors such as users' electricity consumption habits, psychosocial aspects of social activities, and demand response-related behavioral characteristics [12]. By extracting user characteristics, analyzing behaviors, and providing quantitative descriptions, *VPP*s can precisely model user behavior, enabling precise sensing, potential tapping, and value utilization of distributed resources [13]. Taking the modeling of electric vehicle (EV) charging and discharging behavior as an example, the current mainstream modeling approach is based on big data from power networks and transportation networks, using machine learning methods. Reference [14] simulates EV travel, charging, and battery swapping behaviors based on a coupled system of power networks, transportation networks, and information networks. Reference [15] analyzes EV user charging behavior from both macro and micro perspectives, using a multi-source data fusion method that integrates transportation and energy data. Reference [16] characterizes the uncertainty of EV user behavior, based on consumer psychology and social behavior theory. Reference [17] summarizes the modeling methods for EV travel and charging behavior that integrate micro-level driver decisions with macro-level network dynamics. Estimating adjustable response capacity refers to assessing the frequency support capacity that various types of distributed resources aggregated by *VPP*s can provide in each time period. Some of the foundational tasks for *VPP*s are to effectively regulate resources, participate in power market transactions, and provide frequency support ancillary services. Based on theoretical analysis, technical constraints, economic constraints, and availability constraints, the response capacity of *VPP*s is typically classified into four categories: theoretical, technical, economic, and adjustable response capacities [18]. Existing research mostly estimates response capacity from the perspective of load characteristics, believing that demand response capacity depends on user electricity consumption characteristics [19,20]. The upper limit of the response capacity for distributed resources to provide frequency support is the technical response capacity, and when estimating frequency response capacity, it is necessary to consider the requirements of frequency support ancillary services on the performance of distributed resources.

Furthermore, due to the involvement of power flow constraints and integer variables in the scheduling of virtual power plants, the essence of their optimization model becomes a mixed-integer nonlinear programming problem, and finding its optimal solution is a pressing challenge that needs to be addressed. Metaheuristic algorithms are capable of handling complex, nonlinear problems without requiring specific assumptions about the problem's model [21]. They gradually approximate the optimal solution through search and optimization methods, making them excellent at tackling highly complex and uncertain optimization problems [22]. Currently, widely adopted heuristic algorithms include the simulated annealing algorithm [23], ant colony algorithm [24], genetic algorithm [25], particle swarm algorithm [26], and others. Research on these algorithms has yielded some results, but there is still considerable room for improvement in terms of computational speed and accuracy of results [27]. The priority list method is simple and fast, but its results are rough and generally cannot yield the optimal solution. Dynamic programming is a widely used scheduling algorithm, but as the system scale and scheduling time increase, it can easily lead to the curse of dimensionality and make it difficult to consider time-related constraints. The Lagrangian relaxation method cannot robustly handle issues such as oscillations during iteration, obtaining feasible solutions, and convergence conditions during the solution process. The simulated annealing method experiences an exponential increase in computational load when solving larger-scale problems. The ant colony algorithm is prone to premature convergence and getting stuck in local optima. The genetic algorithm is valued for its simplicity, ability to obtain global optimal solutions, and lack of special requirements for the objective function. However, it has a high computational load and low efficiency. The particle swarm algorithm is also prone to getting stuck in local optima, and the accuracy of its solutions is not high enough.

2. Modeling Method for Renewable Energy Uncertainty Based on Interval Error Analysis

2.1. Analysis of the Output Characteristics of Renewable Energy

The output of renewable energy exhibits significant volatility and uncertainty. Taking wind power as an example, its output varies with changes in wind speed and direction, and these changes are characterized by randomness and volatility. Wind speeds fluctuate between near zero and rated wind speeds for most of the year, causing wind power output to fluctuate between zero and rated output. Furthermore, the seasonal characteristics of annual wind power output differ across regions. For instance, in Northeast and North China, the average wind power output is higher in winter and spring and lower in summer and autumn, while in Northwest China, it is the opposite. These differences are primarily due to varying climatic conditions and wind speed patterns in different regions, which increase the difficulty of wind power forecasting for scheduling purposes. The randomness and volatility of wind speeds, along with various factors such as terrain and climate, make it challenging to achieve high-accuracy wind power forecasting. This adds complexity and uncertainty to power system scheduling.

According to grid scheduling requirements, renewable energy power stations must submit short-term power forecasting data to the grid scheduling department every morning, and ultra-short-term power forecasting data at least every hour. Therefore, in this study, the hour is adopted as the time resolution for the short-term power forecasting of renewable energy, and the distribution characteristics of power smoothing by large-scale virtual power plants (*VPP*s) are statistically analyzed. The relative error of power smoothing by large-scale *VPP*s is calculated as follows:

$$e = \frac{W_t^f - W_t}{W_{ed}} \tag{1}$$

In the equation above, W_t^f represents the predicted power value of large-scale virtual power plants used to stabilize renewable energy; W_t denotes the actual power value of large-scale virtual power plants used for the same purpose; and W_{ed} stands for the rated power of the renewable energy power station.

2.2. Confidence Interval for the Uncertainty of Renewable Energy Output

Assuming that the sample data for the prediction error of the power stabilization of renewable energy by a large-scale virtual power plant, obtained after calculating Equation (1), are $e_1, e_2, \ldots, e_n$, where n represents the total number of samples, the kernel density estimate $f(e)$ of the original probability density function for the prediction error of the power stabilization of renewable energy by a large-scale virtual power plant is:

$$f(e) = \frac{1}{nh}\sum_{i=1}^{n} K\left(\frac{e - e_i}{h}\right) \tag{2}$$

In the equation, e_i represents the prediction error of the i-th sample data; h is the bandwidth; and $K(\cdot)$ is the kernel function. Choosing the Gaussian function as the kernel function, its expression is:

$$K\left(\frac{e - e_i}{h}\right) = \frac{1}{\sqrt{2\pi}} \exp\left[-\frac{(e - e_i)^2}{2h}\right] \tag{3}$$

If the confidence interval of the kernel density $f(e)$ shown in Equation (2) follows a normal distribution variable, and at each moment, the confidence level of the large-scale system's dispatchable resources in stabilizing the prediction error of renewable energy is equal, then the confidence level of $f(e)$ must satisfy the renewable energy prediction error interval, as shown in Figure 1.

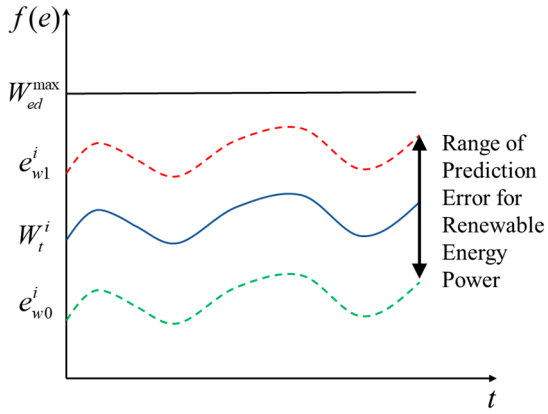


Figure 1. Schematic diagram of renewable energy prediction error interval.

In Figure 1, $W_{ed}^{\max}$ represents the maximum value of $W_{ed}^{\max}$, e_{w0}^i represents the lower bound of the confidence interval for the power prediction error of the i-th sample data of renewable energy mitigated by large-scale controllable resources, and e_{w1}^i represents the upper bound of the confidence interval for the same. Based on the renewable energy prediction error range shown in Figure 1, the actual power value W_t^i mitigated by a large-scale virtual power plant for renewable energy can be expressed as:

$$W_t = W_t^i + e \tag{4}$$

According to Equation (4), combined with the renewable energy prediction error range shown in Figure 1, it can be known that the location confidence interval for the prediction error confidence interval is $[e_{w_0}^i, e_{w_1}^i]$, and the normal distribution that the renewable energy prediction error range follows has a mean of 0 and a variance of S. Since this prediction error follows a standard normal distribution, the standard deviation of $f(e)$ needs to satisfy:

$$\sigma = \sqrt{S} \tag{5}$$

In the equation, σ represents the standard deviation of the normal distribution of the samples for mitigating renewable energy power prediction errors using large-scale virtual energy storage.

By combining Equations (4) and (5), the values of e_{w0}^i and e_{w1}^i can be determined, and their expressions are:

$$\begin{cases} e_{w_0}^i = \max(0, W_t + f^{-1}(1-\varepsilon)) \\ e_{w_1}^i = \min(0, W_t + f^{-1}(\varepsilon)) \end{cases} \tag{6}$$

In the equation, f^{-1} represents the inverse function of the normal probability distribution function; ϵ represents the significance level; and $1-\epsilon$ represents the non-significance level.

By integrating the probability density function of the prediction error, the probability distribution function can be obtained as:

$$F(e) = \int_{-\infty}^{e} f(x)d(x) \tag{7}$$

In the equation, $F(\cdot)$ represents the probability distribution function, and $f(\cdot)$ represents the probability density function.

Based on the values of e_{w0}^i and e_{w1}^i shown in Equation (6), and according to the renewable energy prediction error range, if the value of $F(e)$ falls within the range $(0 < \epsilon < 1)$, the error confidence interval at a confidence level of $1-\epsilon$ is:

$$F(e_{wo}^i \le e \le e_{w1}^i) = 1 - \varepsilon \tag{8}$$

It should be noted that Equation (7) provides the method for calculating the probability distribution function, and is utilized in Equation (8) to compute the error confidence interval. The confidence interval for renewable energy error prediction shown in Equation (8) also follows a normal distribution. Therefore, when the confidence interval shown in Equation (8) reaches the specified confidence level, the interval for the mathematical expectation of the normal distribution of the prediction error samples is:

$$A^{\Delta} - \frac{\sigma}{\sqrt{n}}\delta_{\frac{\varepsilon}{2}} \le \sigma \le A^{\Delta} + \frac{\sigma}{\sqrt{n}}\delta_{\frac{\varepsilon}{2}} \tag{9}$$

In the formula, A^{Δ} represents the sample mean and δ denotes the mathematical expectation of the normal distribution of samples, where large-scale virtual energy storage mitigates renewable energy power prediction errors. By synthesizing the aforementioned formulas, we can obtain ϵ and $1-\epsilon$, and then calculate the confidence level η for the renewable energy power prediction error, according to Equation (10).

$$\eta = 1 - 2\varepsilon \tag{10}$$

At this point, the confidence interval obtained from Equation (10) lies between [e^i_{w0}, e^i_{w1}]. By incorporating the confidence level η calculated using Equation (10) for the predicted power of renewable energy into the scheduling plan, the establishment of a scheduling model for large-scale virtual power plants to mitigate renewable energy power prediction errors can be achieved.

3. Low-Carbon Economic Dispatch Model and Constraints Considering the Participation of Virtual Power Plants

3.1. Carbon Trading Mechanism

Under the carbon trading mechanism, virtual power plants (*VPP*s) can adjust the operation strategies of their internal resources more flexibly to optimize economic dispatch. For instance, when renewable energy generation is sufficient, *VPP*s can increase the proportion of renewable energy output and reduce the use of carbon emission allowances. Conversely, when renewable energy generation is insufficient, *VPP*s can purchase carbon emission allowances to meet production demands, thereby maintaining the stable operation of the power system. The core of the carbon trading mechanism lies in promoting enterprises to actively reduce emissions, by setting an overall cap on carbon emissions and allocating emission allowances. As an energy coordination management system, *VPP*s can achieve emission reduction benefits by optimizing the operation strategies of internal resources to reduce unnecessary carbon emissions. In this paper, the baseline method is adopted for carbon emission allowances, which means that the carbon emission allowance for a *VPP* at a certain time is determined as follows:

$$E_{VPP} = \sum_{m} \psi P_m \tag{11}$$

In the formula, m represents the number of generators in the *VPP*; P_m denotes the output power of generator m at a certain time; and ψ is the emission allocation coefficient per unit of electricity for the *VPP*.

The carbon emissions of a *VPP* originate from the CO_2 generated by gas turbines and electricity purchased from the main grid. The revenue earned from participating in the carbon trading market can be calculated using the following formula:

$$B^c = \lambda_c (E_{VPP} - E_{MT} - E_G) \tag{12}$$

In the formula, λ_c represents the carbon trading price for the *VPP* (virtual power plant); E_{VPP} denotes the carbon emission allowances allocated to the *VPP*; E_{MT} is the carbon emissions produced by the gas turbines; and E_G represents the carbon emissions generated from the electricity purchased by the *VPP* from the main grid.

3.2. Establishment of the Objective Function

This paper aims to establish an objective function that maximizes the economic benefits and minimizes the carbon emissions of the virtual power plant (*VPP*). The objective function is composed of the following components:

Maximization of Economic Benefits for *VPP*

$$F = \max \sum_{s=1}^{N} a(s)(P_G^s + B^s - C^s) \tag{13}$$

In the above equation, F represents the net income of the *VPP*; N is the number of classic scenarios; $\alpha(s)$ is the probability of scenario s occurring; P_G^s is the power generation

revenue of the *VPP* in scenario s; B^s is the carbon trading revenue of the *VPP* in scenario s; and C^s is the cost of the *VPP* in scenario s.

The 24 h power generation revenue of the *VPP* is calculated as follows:

$$P_G^s = \sum_{t=1}^{24} G_{I,t}(P_{pw,t}^s + P_{pv,t}^s + P_{gt,t}^s + P_{dis,t}^s + P_{sell,t}^s - P_{ch,t}^s - P_{buy,t}^s) \tag{14}$$

In the above equation, $G_{I,t}$ represents the electricity selling price at time t; $P_{pw,t}^s$, $P_{pv,t}^s$, and $P_{gt,t}^s$ are the power outputs of wind turbines, photovoltaic systems, and gas turbines, respectively, in scenario s during time period t; $P_{ch,t}^s$ and $P_{dis,t}^s$ are the charging and discharging powers of the electrical energy storage system, respectively, in scenario s during time period t; and $P_{sell,t}^s$ and $P_{buy,t}^s$ are the power sold to and purchased from the grid by the *VPP* in scenario s during time period t, respectively.

$$C^s = C_{op,t}^s + C_{es,t}^s + C_{pu,t}^s \tag{15}$$

$$C_{op,t}^s = \sum_{t=1}^{24} [E_{op,pw}P_{pw,t}^s + E_{op,pv}P_{pv,t}^s + E_{op,gt}P_{gt,t}^s + E_{op,ba}(P_{dis,t}^s - P_{ch,t}^s)] \tag{16}$$

$$C_{es,t}^s = \sum_{t=1}^{24} C_{gt}P_{gt,t}^s \tag{17}$$

$$C_{pu,t}^s = \sum_{t=1}^{24} G_{2,t}\left|D_{n,t} - P_{pw,t}^s - P_{pv,t}^s - P_{gt,t}^s - P_{dis,t}^s\right| \tag{18}$$

In the above equation, $C_{op,t}^s$, $C_{es,t}^s$, and $C_{pu,t}^s$ represent the operational cost, primary energy purchase cost, and electricity curtailment penalty cost of the *VPP* in scenario s during time period t, respectively. $E_{op,pw}$, $E_{op,pv}$, $E_{op,gt}$, and $E_{op,ba}$ are the cost coefficients for wind power, photovoltaic power, gas turbine power generation, and energy storage, respectively. C_{gt} represents the fuel cost of the gas turbine. $G_{2,t}$ is the electricity price at which the *VPP* purchases power from the main grid during time period t. $D_{n,t}$ represents the power that the system can absorb during time period t.

$$C_{gt} = C_{ng}/(\xi L_{ng}) \tag{19}$$

In the above equation, C_{ng} represents the price of natural gas; ξ denotes the power generation efficiency; and L_{ng} is the lower heating value of natural gas.

Capacity plan declared by the *VPP* to the grid:

$$O = \begin{cases} O_{pw} + O_{pv} + \xi P_{gt,\max}, & G_{2,t} \geq G_{gt} \\ O_{pw} + O_{pv}, & G_{2,t} < G_{gt} \end{cases} \tag{20}$$

The carbon emissions generated by the gas turbine within the *VPP*, as well as those resulting from the *VPP*'s electricity purchases from the main grid, are as follows:

$$E_{CO2} = E_{gt} + E_{buy} \tag{21}$$

In the above equation, E_{gt} represents the carbon emissions from the gas turbine and E_{buy} represents the carbon emissions generated from purchasing electricity.

$$E_{gt} = \sum_{s=1}^{N}\sum_{t=1}^{T} [a + bP_{gt,s}^s + c(P_{gt,s}^s)^2] \tag{22}$$

$$E_{buy} = \sum_{s=1}^{N} \sum_{t=1}^{T} P_{buy,t}^{s} \varepsilon_{co2} \sigma_{co2} \tag{23}$$

In the above equation, a, b, and c are the carbon emission coefficients for electricity generation by the gas turbine; ε_{co2} represents the average share of carbon-containing energy sources; and σ_{co2} represents the carbon emission coefficient per kilowatt-hour.

3.3. Constraints

(1) *VPP* Operational Power Balance Constraint

$$\kappa_t + P_{ch,t}^{s} = P_{pw,t}^{s} + P_{pv,t}^{s} + P_{gt,t}^{s} + P_{dis,t}^{s} \tag{24}$$

In the above formula, κ_t represents the power loss when the *VPP* purchases electricity from the main grid during time period t.

(2) Gas Turbine Power Constraint

$$P_{gt,\min} \leq P_{gt,t}^{s} \leq P_{gt,\max} \tag{25}$$

In the above formula, $P_{gt,\min}$ and $P_{gt,\max}$ represent the lower and upper limits of the gas turbine's power, respectively.

(3) Gas Turbine Ramp Rate Constraint

$$-R_{g}^{\min} \Delta t \leq P_{gt,t}^{s} - P_{gt,t-1}^{s} \leq R_{g}^{\max} \Delta t \tag{26}$$

In the above formula, $R_{g}^{\min}$ and $R_{g}^{\max}$ represent the minimum and maximum ramp rates of the gas turbine, respectively; Δt represents the length of one scheduling interval.

(4) Energy Storage System Battery Capacity Constraint

During the scheduling process, the energy storage system must adhere to the law of the conservation of energy, and its constraint condition can be expressed as follows:

$$S_{ch,t}^{s} = S_{ch,t-1}^{s} + \frac{\Delta t (v_1 P_{ch,t}^{s} - P_{dis,t}^{s} / v_2)}{E_{ca}} \tag{27}$$

$$S_{ch,\min}^{s} \leq S_{ch,t}^{s} \leq S_{ch,\max}^{s} \tag{28}$$

In the above formula, $S_{ch,t}^{s}$ and $S_{ch,t-1}^{s}$ represent the capacities of the energy storage battery at time periods t and $t-1$, respectively; v_1 and v_2 represent the charging and discharging efficiencies, respectively; E_{ca} represents the installed capacity of energy storage; and $S_{ch,\max}^{s}$ and $S_{ch,\min}^{s}$ represent the upper and lower limits of the energy storage capacity, respectively.

(5) Energy Storage System Battery Charging and Discharging Constraint

$$\begin{cases} P_{ch,\min} \leq P_{ch,t}^{s} \leq P_{ch,\max} \\ P_{dis,\min} \leq P_{dis,t}^{s} \leq P_{dis,\max} \\ H_{ch,t}^{s} + H_{dis,t}^{s} \leq 1 \end{cases} \tag{29}$$

In the above formula, $P_{ch,\max}$ and $P_{ch,\min}$ represent the upper and lower limits of charging power, respectively; $P_{dis,\max}$ and $P_{dis,\min}$ represent the upper and lower limits of discharging power, respectively; and $H_{ch,t}^{s}$ and $H_{dis,t}^{s}$ represent the charging and discharging states during time period t in scenario s, with values of 0 or 1.

4. Solution Algorithm

4.1. Introduction to the Traditional ALO Algorithm

The problem of economic dispatch in power systems considering the participation of virtual power plants is essentially a mixed-integer nonlinear programming problem with high computational complexity. In some extreme scenarios, it is difficult to search for the optimal solution. Therefore, this paper proposes an improved ant lion Optimizer (ALO) algorithm. The ALO algorithm finds the optimal solution by mimicking the process of antlions constructing traps and preying on ants in nature [28,29]. The ALO algorithm has two populations: one is the ant population, and the other is the antlion population. The five basic modules of the hunting process are the random walking of ants, ants falling into traps, ants sliding towards antlions, antlions capturing ants, and antlions rebuilding traps. The mathematical model of the ALO algorithm starts with random walking in the search space, and can be described as follows:

$$x(t) = \{0, cumsum[2r(t_1) - 1, cumsum[2r(t_2) - 1, \cdots, cumsum[2r(t_n) - 1] \tag{30}$$

$$r(t) = \begin{cases} 1, & if\ rand > 0.5 \\ 0, & if\ rand < 0.5 \end{cases} \tag{31}$$

In the above formula, $x(t)$ represents random walking at the t-th iteration; *cumsum* denotes the cumulative sum; n is the maximum number of iterations; $r(t)$ is a random function; and *rand* represents a random number within [0, 1].

To ensure that the ants move randomly within the search space without exceeding the boundaries, the positions of the ants are adjusted as follows:

$$y_i^t = \frac{(x_i^t - a_i)(d_i^t - c_i^t)}{b_i - a_i} + c_i^t \tag{32}$$

In the above formula, a_i and b_i represent the minimum and maximum values of x_i, respectively, and c_i^t and d_i^t represent the minimum and maximum values of the i-th variable for a certain ant at the t-th iteration, respectively. To simulate the process of ants wandering aimlessly around the antlion and getting trapped, the calculation formula is as follows:

$$c_i^t = Antlionn_i^t + c^t \tag{33}$$

$$d_i^t = Antlionn_i^t + d^t \tag{34}$$

In the above formula, $Antlionn_i^t$ represents the position of the antlion selected by the i-th ant at the t-th iteration. By adaptively reducing the range of random walking of the ants, the process of ants sliding into the antlion's lair is simulated, as shown below:

$$c^t = \frac{c^t}{I} \tag{35}$$

$$d^t = \frac{d^t}{I} \tag{36}$$

In the above formula, I represents a proportional parameter that is dynamically adjusted according to the increase in the number of iterations.

$$I = \begin{cases} 1, t \le 0.1T \\ 10^{\lambda}, t > 0.1T \end{cases} \tag{37}$$

In the above formula, t represents the current number of iterations; T represents the maximum number of iterations; and w is a parameter that is dynamically adjusted based on the number of iterations.

4.2. Principle of Algorithm Improvement

The improvement in this paper lies in the use of a hybrid strategy, combining chaotic mapping and tournament selection to replace the traditional roulette wheel selection method for population initialization. This effectively avoids a situation where too many potential solutions are located at the same boundary point during the optimization process. Based on the random walking mechanism of the ants, a tournament is conducted among individuals randomly selected from the population to select the optimal antlion and elite antlion walks. The positions of the ants are updated in each iteration:

$$Ant_i^t = \frac{R_A^t + R_E^t}{2} \tag{38}$$

In the above formula, Ant_i^t represents the position selected for the i-th ant at the t-th iteration; R_A^t represents the position around the antlion selected through the tournament; and R_E^t represents the random walking of ants around the elite antlion. To initialize the population, Chebyshev chaotic mapping is used for the setup:

$$x_{k+1} = \cos[A \cos^{-1}(x_k)] \tag{39}$$

In the above formula, k represents the number of iterations for the chaotic sequence; A is a mapping coefficient; and $A = 2$ is selected in this paper. During the process of individual selection within the population, the fitness values of each pair of ants and antlions are compared, rather than merging and sorting the ants and antlions. During the comparison, if the fitness value of an ant is better than that of an antlion, the position of the antlion is updated to the position of the ant. The calculation formula is as follows:

$$Antlionn_i^t = Ant_i^t, \ \ if \ f(Ant_i^t) < \ f(Antlionn_i^t) \tag{40}$$

To avoid a situation where too many ants in the population are located at the same boundary point during the optimization process, a random entry into the search space is achieved through Equation (41).

$$Ant_i^t = b_{low} + rand \times (b_{up} - b_{low}) \ if \ Ant_i^t > b_{up} \ \ or \ Ant_i^t < b_{up} \tag{41}$$

In the above formula, b_{low} and b_{up} represent the lower and upper bounds of the search space, respectively.

5. Case Study

To further demonstrate the effectiveness and feasibility of the model and algorithm proposed in this paper, an improved IEEE-30 bus test system is employed for verification [30]. The system structure topology is illustrated in Figure 2 below, where two *VPP*s are connected at buses 7 and 23, large-capacity wind farms are respectively connected at buses 3, 17, and 29, and photovoltaic power plants are integrated into the system through buses 16, 21, and 26. The system structure of the virtual power plants is shown in Figure 3. The division of peak and off-peak time-of-use electricity prices is depicted in Figure 4 below.

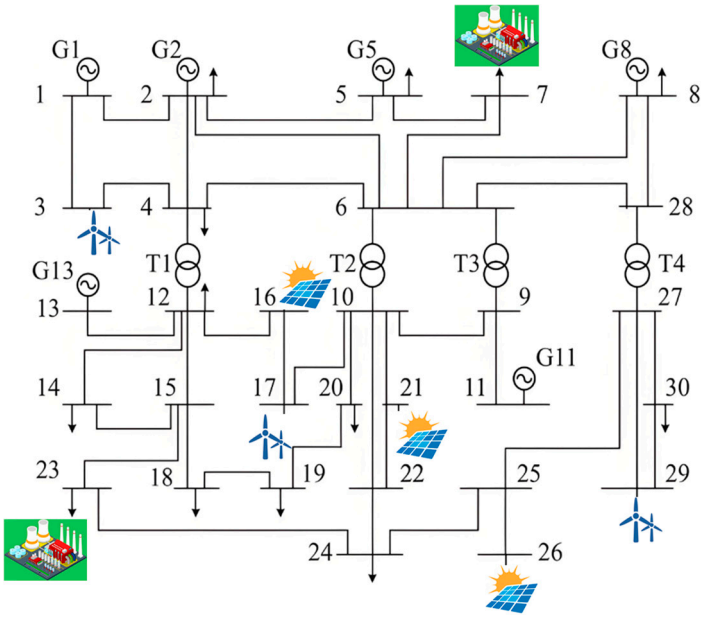


Figure 2. The structure topology of improved IEEE-30 bus test system.

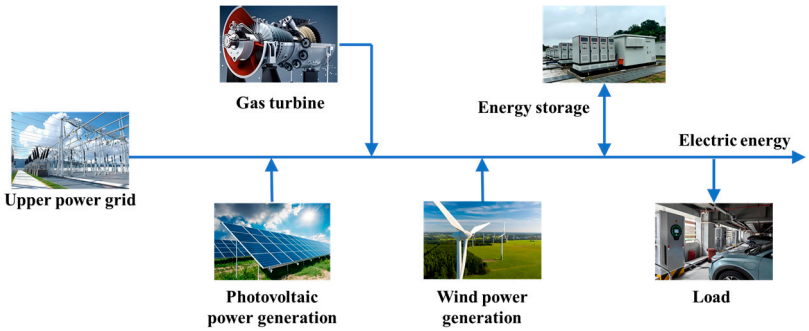


Figure 3. The structure topology of *VPP*s.

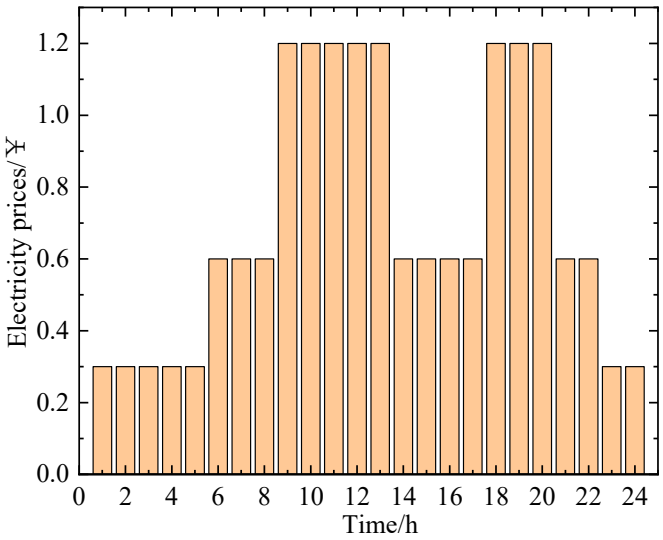


Figure 4. The division of peak and off-peak time-of-use electricity prices.

5.1. Analysis of Low-Carbon Benefits

Two operational modes are established based on whether the carbon trading mechanism is considered, and the net benefits and carbon emissions of the *VPP* under different modes are shown in Table 1. It can be observed that when carbon trading is taken into

account, the net profit of the *VPP* increases while carbon emissions decrease, indicating that the *VPP* model considering carbon trading balances both economic efficiency and environmental protection. Specifically, in the mode without considering carbon trading, the *VPP* mainly focuses on the direct economic benefits of its electricity production and sales, i.e., electricity sales revenue minus electricity production costs. Due to the absence of a carbon trading mechanism, the *VPP* has no incentive to reduce carbon emissions, because it does not gain direct economic benefits from such reductions. Therefore, in this mode, the *VPP* may tend to adopt less costly but higher carbon generation methods to maximize its net profit.

Table 1. Comparison of carbon emissions and operating costs across different modes.

VPP Operation Modes	Carbon Emissions/kg	Operating Cost/¥
Mode 1: Considering Carbon Trading	2547.6	8452.1
Mode 2: Without Considering Carbon Trading	3254.4	9625.7

Next, let us consider a scenario where a carbon trading mechanism is introduced. This mechanism allows carbon emission permits to be traded as a commodity, converting carbon emissions into economic value. When the *VPP* reduces its carbon emissions, it can sell surplus carbon emission quotas to entities that require more quotas, thereby obtaining additional economic benefits. This mechanism incentivizes the *VPP* to adopt more environmentally friendly generation methods and reduce carbon emissions, to gain greater profits in the carbon trading market. When the *VPP* considers carbon trading, it weighs up the costs and carbon emissions of different generation methods. If a certain generation method has lower carbon emissions but slightly higher costs, the *VPP* may choose this method because it can offset the cost increase by selling carbon emission quotas, or even obtain additional profits. In this way, the net profit of the *VPP* increases while carbon emissions decrease.

Observing Figure 5, it can be found that under the carbon trading mechanism, the carbon emissions per unit of electricity generated by gas turbines, as carbon emission sources, become a factor to consider. To reduce carbon emission costs, gas turbines may actively decrease their electricity generation, especially when the price of carbon emission permits is high. Gas turbines may adopt optimized scheduling strategies, such as adjusting the power generation load curve and improving generation efficiency, to reduce their carbon emission intensity. The output of gas turbines will be shifted from peak hours to off-peak hours, to avoid cost increases during peak hours due to high electricity prices and high carbon emission permit prices. As adjustable loads such as electric vehicles increase, the output of gas turbines may be further suppressed, because electric vehicles can choose to charge using renewable energy electricity, thereby reducing dependence on traditional fossil fuels. The output level of gas turbines may also be directly affected by carbon trading prices. The higher the carbon trading price, the greater the incentive for gas turbines to reduce their output, as this can lower carbon emissions and thus reduce carbon emission costs. Under the carbon trading mechanism, if the output of gas turbines decreases, *VPP*s need to purchase more electricity from the upper-level grid to meet electricity demand. Especially during periods of insufficient renewable energy generation or peak electricity usage, *VPP*s may increase their purchases from the upper-level grid. When purchasing electricity, *VPP*s may pay more attention to the low-carbon and economic attributes of the power. Therefore, in terms of purchasing structure, they may prefer to buy renewable energy electricity or low-carbon electricity. This will help reduce the overall carbon emissions of *VPP*s and

increase their economic benefits. The introduction of the carbon trading mechanism will prompt *VPP*s to participate more actively in electricity market transactions. Optimizing the electricity purchasing structure and reducing purchasing costs through market means will be one of the most important strategies for *VPP*s.

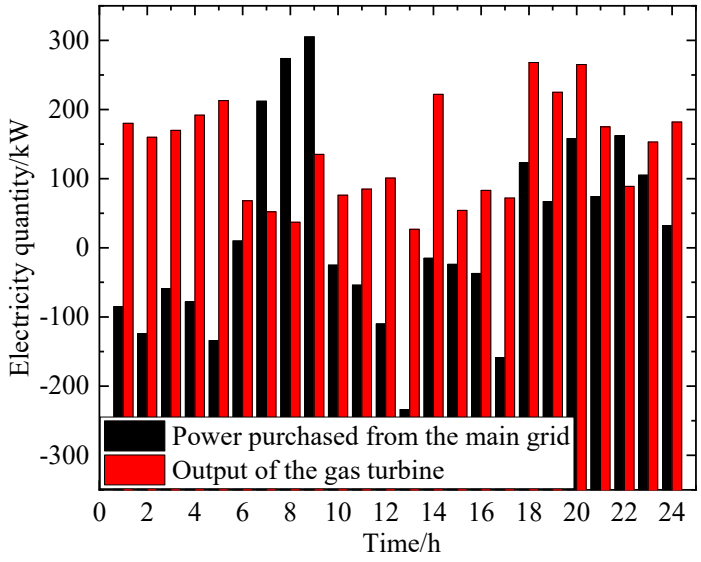


Figure 5. Output of power units and electricity purchased from the grid.

5.2. Optimality Verification of the Scheduling Model

Figure 6 presents wind and solar curtailment rates under different scheduling strategies. It can be observed that using error intervals to characterize the uncertainty of renewable energy output achieves lower wind and solar curtailment rates compared to multi-scenario-based stochastic optimization (method A) [31], fuzzy chance constraint-based stochastic optimization (method B) [32], and traditional robust optimization (method C) [33]. The error interval method, by calculating the prediction error distribution of renewable energy output, can more accurately depict the range of uncertainty in renewable energy output. Figure 7 further demonstrates the economic benefits and computational efficiency of different methods. In Figure 6, the wind and solar curtailment rates for the proposed method, Method A, Method B, and Method C are 6.24%, 7.26%, 8.48%, and 9.01%, respectively. Through the calculation of confidence intervals, the uncertainty range of renewable energy output can be more precisely described, enabling a more accurate assessment of various possible output scenarios during economic dispatch. This precision aids in formulating more reasonable dispatch strategies and reducing the phenomenon of wind and solar power curtailment due to fluctuations in renewable energy output. Converting uncertainty optimization problems into deterministic optimization problems simplifies the calculation process and reduces computational complexity. Additionally, deterministic optimization problems typically have a clearer solution space, facilitating the discovery of global optimal or near-optimal solutions. Traditional robust optimization algorithms often analyze based on the worst-case scenario, assuming that renewable energy output reaches its maximum uncertainty boundary. This conservative strategy tends to lead to overly conservative dispatch strategies, thereby increasing the risk of wind and solar power curtailment. Scenario-based stochastic optimization algorithms simulate the uncertainty of renewable energy output by generating multiple possible scenarios. However, this method may be limited by the number and representativeness of scenarios, leading to inaccurate optimization results. Fuzzy chance-constrained optimization algorithms consider the fuzziness of renewable energy output and allow constraint violations within a certain probability.

Nevertheless, this method may struggle to accurately assess the actual uncertainty range of renewable energy output, thereby affecting the accuracy of the optimization results.

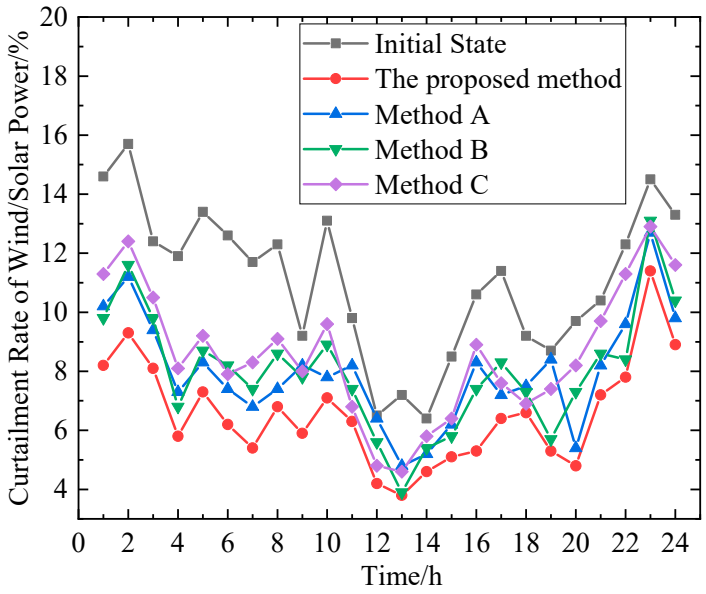


Figure 6. Comparison of wind/solar power curtailment rates under different scheduling strategies.

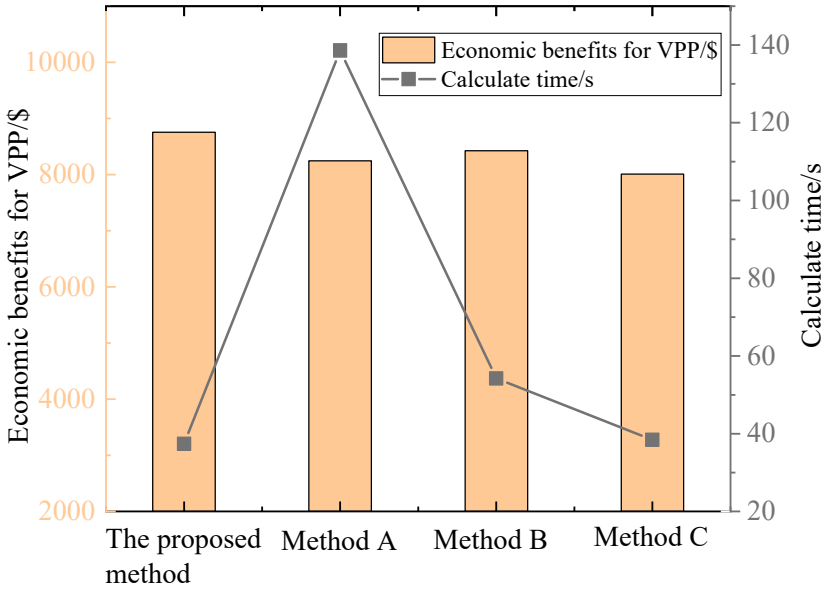


Figure 7. Comparison of economic indicators and computational efficiency among different methods.

Observing the above figure, it can be seen that the core of the proposed method lies in converting the originally complex and difficult-to-solve uncertainty optimization problem into a more manageable deterministic optimization problem, through confidence interval calculation and transformation. Compared to other methods, the economic income can be increased by up to 3.2%, and the computation time is only 12.5% of that required for scenario screening-based stochastic optimization. Confidence interval calculation allows decision-makers to set a confidence level according to their own risk appetite, thereby maximizing the economic income of the *VPP* while ensuring a certain level of risk. This method offers more a flexible balancing of risk and return compared to robust optimization (which tends to adopt conservative strategies to address worst-case scenarios) and stochastic optimization (which may underestimate or overestimate risks due to improper scenario selection). On the other hand, the confidence interval can quantify the uncertainty

range of renewable energy output, enabling more precise scheduling plans to be developed accordingly. Compared to fuzzy chance-constrained optimization, the confidence interval provides clearer boundary conditions, helping to reduce decision-making errors caused by fuzziness. The proposed method allows for optimization under a wider range of conditions, not limited to specific scenarios or worst-case scenarios, potentially enabling the discovery of scheduling solutions with higher economic value. In terms of computational efficiency, the proposed method converts the uncertainty optimization problem into a deterministic one, significantly reducing the complexity of the model. Compared to stochastic optimization, which requires simulating multiple scenarios, and fuzzy optimization, which deals with the complexity of fuzzy sets, the confidence interval method avoids these additional computational burdens. Due to the model simplification, the confidence interval method may not require repeated iterations to verify the robustness of the solution, as robust optimization does, nor does it need to solve each scenario separately, as stochastic optimization does, thereby reducing the total computation time.

Additionally, this paper compares the proposed algorithm with other conventional solution algorithms. The test data were sourced from the CEC 2017 benchmark suite, encompassing unimodal functions, multimodal functions, and hybrid functions. The algorithms were evaluated and compared based on average error, average convergence time, and Wilcoxon rank-sum test results. The relevant results are presented in Table 2 below.

Table 2. Effectiveness comparison of different algorithms.

Index	The Improved ALO	ALO	PSO	GA	MS-TSA	I-CPA
References for methods	/	[29]	[34]	[35]	[36]	[37]
Average error/%	2.57%	3.79%	3.26%	3.88%	2.74%	2.99%
Average convergence time/s	52.4	60.2	65.8	69.2	59.7	62.3
Wilcoxon rank-sum	1	4	5	6	2	3

Observing the table above, it can be found that the improved ALO algorithm optimizes the initialization process of the population by introducing a hybrid strategy of chaotic mapping and tournament selection. Chaotic mapping is able to generate a more diverse and uniformly distributed initial population, which helps the algorithm better explore the global optimal solution in the search space. The tournament selection method further enhances the competitiveness and diversity of the population, aiding the algorithm in avoiding premature convergence during the iteration process. These optimization measures enable the improved ALO algorithm to more accurately find the global optimal solution when solving complex optimization problems, thereby reducing the average error. In terms of convergence speed, the improved ALO algorithm also performs well. The introduction of chaotic mapping allows the algorithm to quickly converge to an appropriate solution in the early stages of iteration, while the tournament selection method helps the algorithm continuously optimize the quality of the solution during the iteration process. Additionally, the improved ALO algorithm combines the inherent advantages of the ant lion optimizer, such as mimicking the antlion's predation mechanism for random walks and trap construction. These characteristics endow the algorithm with stronger adaptability and robustness during the search process. Therefore, the improved ALO algorithm can achieve convergence in a shorter period of time, reducing the average convergence time. Furthermore, the Wilcoxon rank-sum test is a non-parametric test method used to compare the positions or medians of two independent samples. In the evaluation of algorithm performance, the Wilcoxon rank-sum test can be used to test whether the differences between the results obtained by different algorithms when solving the same optimization problem are significant. The improved ALO algorithm performs optimally in terms of the Wilcoxon

rank-sum test, indicating that its results have significant advantages compared to those of other algorithms. This further validates the effectiveness and superiority of the improved ALO algorithm in solving complex optimization problems.

The size of the test system also has an impact on the final dispatch results. The improved IEEE-118 bus test system has been adopted for further verification Figure 8. The structure of the test system is shown in the figure below.

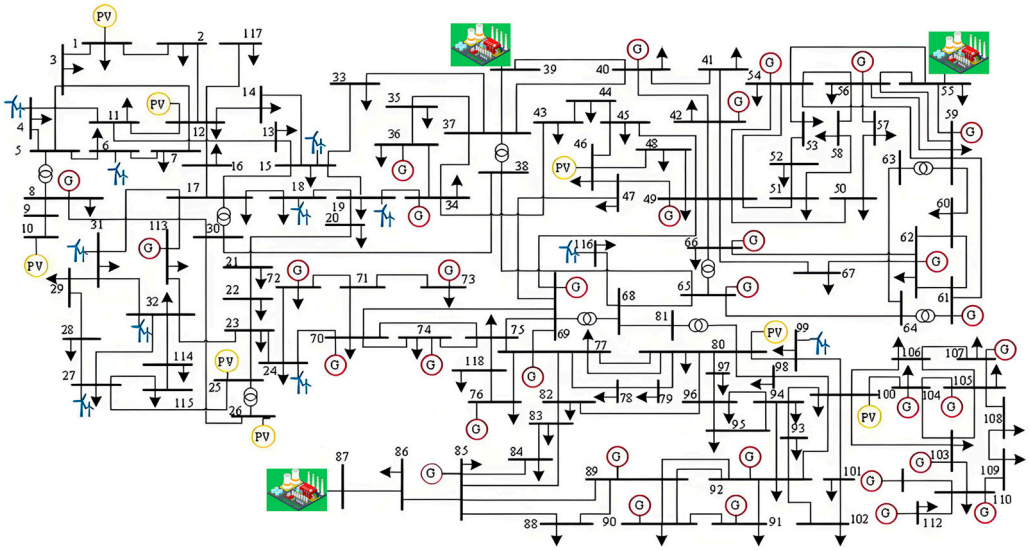


Figure 8. The structure topology of improved IEEE-118 bus test system.

After calculation, the economic indicators and computation time are presented in Table 3. It can be observed that the proposed method maintains high computational efficiency and economic benefits, even in large-scale test systems. By accurately quantifying the uncertainty of renewable energy generation, the confidence interval method can maximize the economic benefits of virtual power plants, while ensuring the safe and stable operation of the power grid. In large-scale test systems, this method can more accurately capture the volatility and randomness of renewable energy generation, thereby formulating better economic dispatch strategies and increasing the total revenue of virtual power plants. By setting a confidence level, the confidence interval method can tolerate a certain degree of uncertainty in renewable energy generation, enhancing the robustness of virtual power plants. Even when there are significant fluctuations in renewable energy generation in large-scale test systems, this method can maintain the stable operation of virtual power plants and reduce economic losses caused by uncertainty. Additionally, it is noteworthy that in large-scale test systems, the computation time of the method proposed in this paper can still be kept within 5 min, meeting the requirements of real-time online calculation and dispatch in power systems.

Table 3. Performance comparison among different methods.

Method	Carbon Emissions/kg	Operating Cost/$	Computation Time/s	Average Wind/Solar Curtailment Rate
The proposed method	5745.6	15862.4	57.4	2.57%
Method A	5975.1	16247.2	625.6	3.52%
Method B	6123.8	17524.9	59.2	3.74%
Method C	6245.1	17996.3	61.3	4.45%

This precise depiction helps the scheduling system gain a more accurate understanding of the actual generation capacity of renewable energy, thereby formulating more reasonable scheduling plans. Compared to multi-scenario stochastic optimization, the error interval method does not require presetting multiple possible generation scenarios, thus avoiding the risk of missing extreme situations due to improper scenario setting. At the same time, it also mitigates the issue of increased computational complexity caused by an excessive number of scenarios. The error interval method allows the scheduling system to flexibly adjust based on the actual prediction error range of renewable energy output. When the prediction error range is large, the scheduling system can correspondingly increase reserve capacity, or adjust the output of other units to ensure the stable operation of the power system. Since the error interval method can more accurately reflect the uncertainty of renewable energy output, it helps reduce wind and solar curtailment caused by this uncertainty. The scheduling system can formulate more precise scheduling strategies based on error intervals, enabling a more full utilization of renewable energy generation. Compared to traditional robust optimization, the error interval method typically does not require complex optimization calculations. It only needs to calculate the prediction error distribution of renewable energy output, based on historical data and prediction models, and then make scheduling decisions based on this distribution. This method has higher computational efficiency and can quickly respond to real-time changes in the power system. The error interval method is applicable not only to the optimal scheduling of large-scale power systems, but also to small- and medium-sized power systems. It can provide effective scheduling strategies for power systems of different scales, helping them achieve more economical, efficient, and reliable operation.

In real-world applications, the fields where the method proposed in this paper can be applied include: (1) High-penetration renewable energy generation areas. In regions with high penetration of renewable energy sources such as wind and solar power, grid dispatch faces significant challenges, due to the randomness and intermittency of renewable energy generation. These areas are often located in remote regions with relatively weak grid structures, and the large-scale integration of renewable energy generation further exacerbates grid instability. By constructing a *VPP*, decentralized renewable energy generation resources, energy storage equipment, and demand-side response resources can be integrated into a virtual entity to participate in the electricity market and grid operation. Utilizing the robust economic management strategy proposed in this paper, effective management of the uncertainty associated with renewable energy generation can be achieved, enhancing the flexibility and economy of the power grid. (2) Optimal dispatch of urban power grids. In urban power grids, due to high load density and diverse electricity demands, grid dispatch requires greater precision and intelligence. At the same time, urban power grids often contain a large amount of distributed energy resources (such as rooftop photovoltaics and small wind turbines) and demand-side response resources (such as electric vehicles and smart buildings). By integrating these resources through a *VPP* and utilizing the improved ALO algorithm proposed in this paper for economic dispatch, optimal dispatch of the urban power grid can be achieved. This not only improves the economy of the power grid, but also reduces carbon emissions, enabling a green and low-carbon energy transition.

6. Conclusions

This paper addresses the new challenges faced by grid security and scheduling in the context of rapid advancements in new energy technologies. It proposes a robust economic management strategy for power systems that considers the participation of *VPP*s. By integrating distributed energy resources and demand-side response resources,

*VPP*s participate in the electricity market and grid operation as virtual entities, effectively enhancing the flexibility and economy of the power system.

The paper first characterizes the uncertainty of renewable energy output through prediction deviations and establishes economic dispatch and constraint conditions for *VPP*s. Given the nonlinear characteristics of the model, an improved ALO algorithm is employed to ensure optimal solutions are obtained. Finally, a case study using an improved IEEE 30-bus test system validates the effectiveness and feasibility of the proposed method. The research results indicate that this method maximizes economic benefits while ensuring the safe and stable operation of the power grid.

Future research can further explore optimal allocation strategies for different types of distributed energy resources and demand-side response resources within *VPP*s, to improve their overall economy and flexibility. By considering renewable energy prediction errors and the uncertainty of demand-side response across different time scales, more refined *VPP* scheduling strategies can be studied to better meet the actual operational needs of the power grid.

Author Contributions: Conceptualization, X.L., C.Z., Q.Y. and J.X.; software, X.L., C.Z., Q.Y. and J.X.; writing—original draft preparation, X.L., C.Z., Q.Y. and J.X. All authors have read and agreed to the published version of the manuscript.

Funding: This research received no external funding.

Data Availability Statement: The original contributions presented in this study are included in the article. Further inquiries can be directed to the corresponding authors.

Conflicts of Interest: Author Chen Zhang was employed by the State Grid Energy Research Institute Co., Ltd., and author Qianqian Yi was employed by Bishan Power Supply Branch of State Grid Chongqing Electric Power Company. The remaining authors declare that the research was conducted in the absence of any commercial or financial relationships that could be construed as a potential conflict of interest.

References

1. Wang, C.; Shi, Z.; Liang, Z. Key Technologies and Prospects for Utilization of Demand-Side Resources in a Renewable Energy-Dominated Power System. *Autom. Electr. Power Syst.* **2021**, *45*, 37–48.
2. Ge, X.; Fu, Z.; Xu, F. Business Models and Key Technologies of Virtual Power Plants for the New-Type Power System. *Autom. Electr. Power Syst.* **2022**, *46*, 129–146.
3. Cao, W.; Qin, H.; Lu, J. Positioning and Application Prospects of Virtual Synchronous Machines in the New-Type Power System. *Autom. Electr. Power Syst.* **2023**, *47*, 190–207.
4. Shimon, A.; Alistair, P. *The Virtual Utility*; Springer: Boston, MA, USA, 1997.
5. Bignucolo, F.; Caldon, R.; Prandoni, V.; Spelta, S.; Vezzola, M. The Voltage Control on MV Distribution Networks with Aggregated DG Units. In Proceedings of the 41st International Universities Power Engineering Conference, Newcastle upon Tyne, UK, 6–9 September 2023; pp. 187–192.
6. Pudjianto, D.; Ramsay, C.; Strbac, G. Virtual power plant and system integration of distributed energy resources. *IET Renew. Power Gener.* **2024**, *1*, 10–16. [CrossRef]
7. Babaei, S.; Zhao, C.; Fan, L. A Data-Driven Model of Virtual Power Plants in Day-Ahead Unit Commitment. *IEEE Trans. Power Syst.* **2019**, *34*, 5125–5135. [CrossRef]
8. Hrvoje, P.; Igor, K.; Tomislav, C. Virtual Power Plant Mid-Term Dispatch Optimization. *Appl. Energy* **2023**, *101*, 134–141.
9. Zhao, H.; Wang, X.; Wang, B.; Ning, B.; Pan, Z.; Sun, H.; Xue, Y. Cloud-Cluster Hierarchical Dispatch for Large Scale Demand-Side Distributed Resources. In Proceedings of the 2021 IEEE 5th Conference on Energy Internet and Energy System Integration, Taiyuan, China, 22–24 October 2021; pp. 272–276.
10. Wang, X.; Liu, D.; Liu, Z.; Liu, M.; Wang, J.; Gao, Y.; Song, Y. Operation Mechanism and Key Technologies of Virtual Power Plant under Ubiquitous Internet of Things. *Power Syst. Technol.* **2019**, *43*, 3175–3183.
11. Bao, P.; Zhang, W.; Zhang, Y. Secondary Frequency Control Considering Optimized Power Support From Virtual Power Plant Containing Aluminum Smelter Loads Through VSC-HVDC Link. *J. Mod. Power Syst. Clean Energy* **2023**, *11*, 355–367. [CrossRef]

12. Xu, X.; Li, K.; Wang, F.; Mi, Z.; Jia, Y.; Wei, W.; Jing, Y. Evaluating Multi-Time Scale Response Capability of EV Aggregator Considering Users' Willingness. *IEEE Trans. Ind. Appl.* **2023**, *57*, 3366–3376. [CrossRef]
13. Chen, Q.; Lv, R.; Guo, H. Modeling of Power Users' Behavior Oriented to Demand Response: Research Status and Applications. *Electr. Power Autom. Equip.* **2023**, *43*, 23–37.
14. Fu, Z.; Zhu, W.; Zhu, J. EV Swapping Demand Forecasting and Charging Optimization Strategy for EV Swapping Stations under the "Vehicle-Electricity-Road-Station" Interconnection. *Electr. Power Autom. Equip.* **2024**, *42*, 116–124.
15. Sheng, Y.; Guo, Q.; Liu, M. Analysis of User Charging Behavior Based on Multi-Source Data Fusion and Planning Practice of Charging Facilities. *Autom. Electr. Power Syst.* **2024**, *46*, 151–162.
16. Hu, J.; Ma, W.; Xue, Y. Quantification of Reserve Capacity for Electric Vehicle Aggregators Based on the CPSSE Framework. *Autom. Electr. Power Syst.* **2022**, *46*, 46–54.
17. Sheng, Y.; Guo, Q.; Xue, Y. Modeling and Collaborative Optimization of Power-Transportation Coupled Networks from the Cyber-Physical-Social Perspective [J/OL]. *Autom. Electr. Power Syst.* **2024**. *ahead of print*.
18. Wang, F.; Li, M.; Zhang, X. Assessment Methods, Applications, and Prospects of Demand Response Resource Potential. *Autom. Electr. Power Syst.* **2023**, *47*, 173–191.
19. Song, M.; Sun, W.; Wang, Y.; Shahidehpour, M.; Li, Z.; Gao, C. Hierarchical Scheduling of Aggregated TCL Flexibility for Transactive Energy in Power Systems. *IEEE Trans. Smart Grid* **2019**, *11*, 2452–2463. [CrossRef]
20. Sun, Y.; Mao, Y.; Li, Z. Comprehensive Clustering Method for User Load Characteristics and Adjustable Potential Oriented to Big Data in Electric Power. *Proc. CSEE* **2024**, *41*, 6259–6270.
21. Beşkirli, A.; Dağ, İ. An efficient tree seed inspired algorithm for parameter estimation of Photovoltaic models. *Energy Rep.* **2022**, *8*, 291–298. [CrossRef]
22. Beşkirli, M.; Kiran, M.S. Optimization of Butterworth and Bessel Filter Parameters with Improved Tree-Seed Algorithm. *Biomimetics* **2023**, *8*, 540. [CrossRef]
23. Huo, X.; Yu, J.; Pang, C.; Ding, Y.; Zhang, J.; Zhao, C.; Yu, B. Integrated Demand Response Optimization for Consumer With Herd Mentality: A Genetic Simulated Annealing Approach. *IEEE Access* **2024**, *12*, 69097–69111. [CrossRef]
24. Xia, K.; Li, Y.; Zhu, B. Improved Photovoltaic MPPT Algorithm Based on Ant Colony Optimization and Fuzzy Logic Under Conditions of Partial Shading. *IEEE Access* **2024**, *12*, 44817–44825. [CrossRef]
25. Li, L.; Wang, Y.; Hu, H.; Ning, H.; Li, X. Design of Energy Internet Power Information Management System Based on Genetic Algorithm. In Proceedings of the 2024 3rd International Conference on Artificial Intelligence and Autonomous Robot Systems (AIARS), Bristol, UK, 29–31 July 2024; pp. 14–19.
26. Halwani, S.; Tawfik, H.; Dahrouj, H.; Elnady, A. Comparative Analysis of Genetic Algorithm and Particle Swarm Opti-mization for Optimal Power Flow on IEEE 30-Bus System. In Proceedings of the 2024 Advances in Science and Engineering Technology Interna-tional Conferences (ASET), Abu Dhabi, United Arab Emirates, 21–22 December 2024; pp. 1–6.
27. Wu, B.; Wang, Z.; Jiang, J. Research on Maximum Power Point Tracking Technology of Adaptive Particle Swarm Optimization Based on Greedy Strategy. In Proceedings of the 2024 IEEE 2nd International Conference on Control, Electronics and Computer Tech-nology (ICCECT), Jilin, China, 26–28 April 2024; pp. 1422–1425.
28. Das, T.; Boruah, N.; Patra, S.; Borah, A.A. Enhanced parameter optimization of PID controller for single area power system using hybrid ALO-GBO algorithm. In Proceedings of the 2024 6th International Conference on Energy, Power and Environment (ICEPE), Shillong, India, 20–22 June 2024; pp. 1–6.
29. Shi, Y.; Zhang, W.; Sang, F.; Zhao, L.; Wang, T. Application of ALO-ELM on Electricity Demand Forecasting under Spot Power Market. In Proceedings of the 2022 4th International Conference on Smart Power & Internet Energy Systems (SPIES), Beijing, China, 27–30 October 2022; pp. 2194–2197.
30. Available online: https://download.csdn.net/download/LF2827417795/90128514 (accessed on 10 November 2024).
31. Cao, Y.; Mu, Y.; Jia, H.; Yu, X.; Hou, K.; Wang, H. A Multi-Objective Stochastic Optimization Approach for Planning a Multi-Energy Microgrid Considering Unscheduled Islanded Operation. *IEEE Trans. Sustain. Energy* **2024**, *15*, 1300–1314. [CrossRef]
32. Ma, R.; Li, X.; Gao, W.; Lu, P.; Wang, T. Random-Fuzzy Chance-Constrained Programming Optimal Power Flow of Wind Integrated Power Considering Voltage Stability. *IEEE Access* **2020**, *8*, 217957–217966. [CrossRef]
33. Zhuang, K.; Wang, Z.; Yang, N.; Xia, K.; Shi, R. Robust Optimization-Driven Strategy for Dynamic Planning of Power Transmission Networks. In Proceedings of the 2024 3rd International Conference on Energy and Electrical Power Systems (ICEEPS), Guangzhou, China, 14–16 July 2024; pp. 617–620.
34. Zhang, H.; Guo, X.; Zhang, P. Improved PSO-SVM-Based Fault Diagnosis Algorithm for Wind Power Converter. *IEEE Trans. Ind. Appl.* **2024**, *60*, 3492–3501. [CrossRef]
35. Xu, H.; Yu, T.; Ren, C.; He, S. Finite-Time Decentralized Sliding Mode Control for Interconnected Systems and Its Application to Electrical Power Systems: A GA-Assisted Design Method. *IEEE Trans. Circuits Syst. I Regul. Pap.* **2024**, *71*, 2835–2847. [CrossRef]

36. Sathish, K.R.; Ananthapadmanabha, T. Power Quality Enhancement in Distribution System Integrated with Renewable Energy Sources Using Hybrid RBFNN-TSA Technique. In Proceedings of the 2021 7th International Conference on Electrical Energy Systems (ICEES), Virtual, 11–13 February 2021; pp. 189–194.
37. Ng, J.S.; Chen, J.; Kyaw, N.A.; Lwin, N.K.Z.; Ho, W.G.; Chong, K.S.; Gwee, B.H. A Highly Efficient Power Model for Correlation Power Analysis (CPA) of Pipelined Advanced Encryption Standard (AES). In Proceedings of the 2020 IEEE International Symposium on Circuits and Systems (ISCAS), Seville, Spain, 12–14 October 2020; pp. 1–5.

Disclaimer/Publisher's Note: The statements, opinions and data contained in all publications are solely those of the individual author(s) and contributor(s) and not of MDPI and/or the editor(s). MDPI and/or the editor(s) disclaim responsibility for any injury to people or property resulting from any ideas, methods, instructions or products referred to in the content.